Electronic Supplementary Material (ESI) for Journal of Materials Chemistry A.
This journal is © The Royal Society of Chemistry 2023

Supporting Information

Role of Cavities Created by Azobenzene-modified UiO-66 in Bulky Ionic Liquid for High Photoresponsive CO_2 Uptake Behavior

Meng-Meng Li,[a] Manish Kumar Dinker,[a] Yang Liu,[a] Mingrui Zuo,[b] Lifeng Ding,[b*] Xiao-Qin Liu,[a] Lin-Bing Sun[a]*

[a]State Key Laboratory of Materials-Oriented Chemical Engineering, Jiangsu National Synergetic Innovation Center for Advanced Materials (SICAM), College of Chemical Engineering, Nanjing Tech University, Nanjing 211816, China.

[b]Department of Chemistry, Xi'an JiaoTong-Liverpool University, Suzhou 215123, China.

*Corresponding author. lbsun@njtech.edu.cn; Lifeng.Ding@xjtlu.edu.cn

Section 1. Supporting Text

Synthesis of pristine UiO-66

The synthesis of UiO-66 was carried out as per the previous report.[1] In a 50 mL vial, 0.4 mmol of $ZrCl_4$ was added in a mixture of 10 mL DMF and 0.3 mL acetic acid as the modulator, and the entire solution was stirred for 10 min to dissolve the metal precursor. Next, 0.4 mmol of terephthalic acid (H_2BDC) was added and dissolved in the solution. The solution was then transferred into a Teflon-lined autoclave and heated for 36 h at 120 °C. After cooling down to room temperature, the precipitate was collected by centrifugation at 6000 rpm from the parent solution. The product was then washed three times with fresh DMF (15 mL) and methanol (15 mL), and further activated at 110 °C under vacuum to obtain white solids (UiO-66).

Molecular Dynamic Simulation Studies

Molecular dynamics (MD) simulations of Azo-UiO-66 cluster cage interacting with an IL molecule were conducted using the Forcite module in Accelrys Materials Studio 7.0 software. The UiO-66-azo cluster was created from the Azo-UiO-66 crystal structure. Four Zr-cluster secondary building units are connected by six ligands forming the Azo-UiO-66 cluster cage. The unconnected carbon atoms of the Zr-cluster secondary building units are terminated by hydrogen atoms. The initial configuration of the MD simulation was constructed with one Azo-UiO-66 cluster cage and one IL molecule that contain one organic ligand with +2 charge and two anions in a cubic box (3.5 nm x 3.5 nm x 3.5 nm). Universal forcefield (UFF) along with charge equilibration method (Q_{eq}) methods were used in the MD simulation.[2] The NVT ensemble with a constant temperature of 298 K was chosen to perform both the initialization and production run. A cut off distance of 1.28 nm was used. The time step and total production run were set as 1.0 fs and 10 ns, respectively. Radial distribution functions analysis was performed between the centroid of the cage and the two terminal carbon atoms of the cationic IL molecule and the two nitrogen atoms of the two IL anions.

Grand Canonical Monte Carlo (GCMC) Simulations

For Grand Canonical Monte Carlo (GCMC) simulations, five random configurations of Azo-UiO-66 cage along with the IL chain were taken from the MD production run. The configurations were treated to be rigid and further used. GCMC simulations of pure CO_2 uptake (298 K, 1 bar) were performed using RASPA 2.0.[3] The point charges of the frameworks were calculated using the charge equilibration method. The interactions between CO_2 and Azo-UiO-66-IL were calculated as a sum of Lennard-Jones (LJ) interactions and Coulomb potentials (Equation 1).

$$\boldsymbol{U(r_{ij}) = 4\epsilon_{ij}[(\frac{\sigma_{ij}}{r_{ij}})^{12} - (\frac{\sigma_{ij}}{r_{ij}})^{6}] + \frac{q_i q_j}{4\pi\epsilon_0 r_{ij}}} \qquad (\mathbf{1})$$

DREIDING was used for the frameworks. The partial charges and LJ parameters of CO_2 were taken from Transferable Potentials for Phase Equilibria (TraPPE) model. Commonly used Lorentz−Berthelot mixing rules were applied for cross interactions of LJ interaction pairs. Ewald summation was used for Coulomb potentials. The spherical cut-off radius was of 1.28 nm. In simulation process, every GCMC simulation consisted of 200,000 initialization cycles for equilibration, followed by 200,000 cycles production run. Density VTK profiles were written per 100 cycles. Density plots were based on overlapping VTK profiles from the GCMC.

Section 2. Supporting Figures

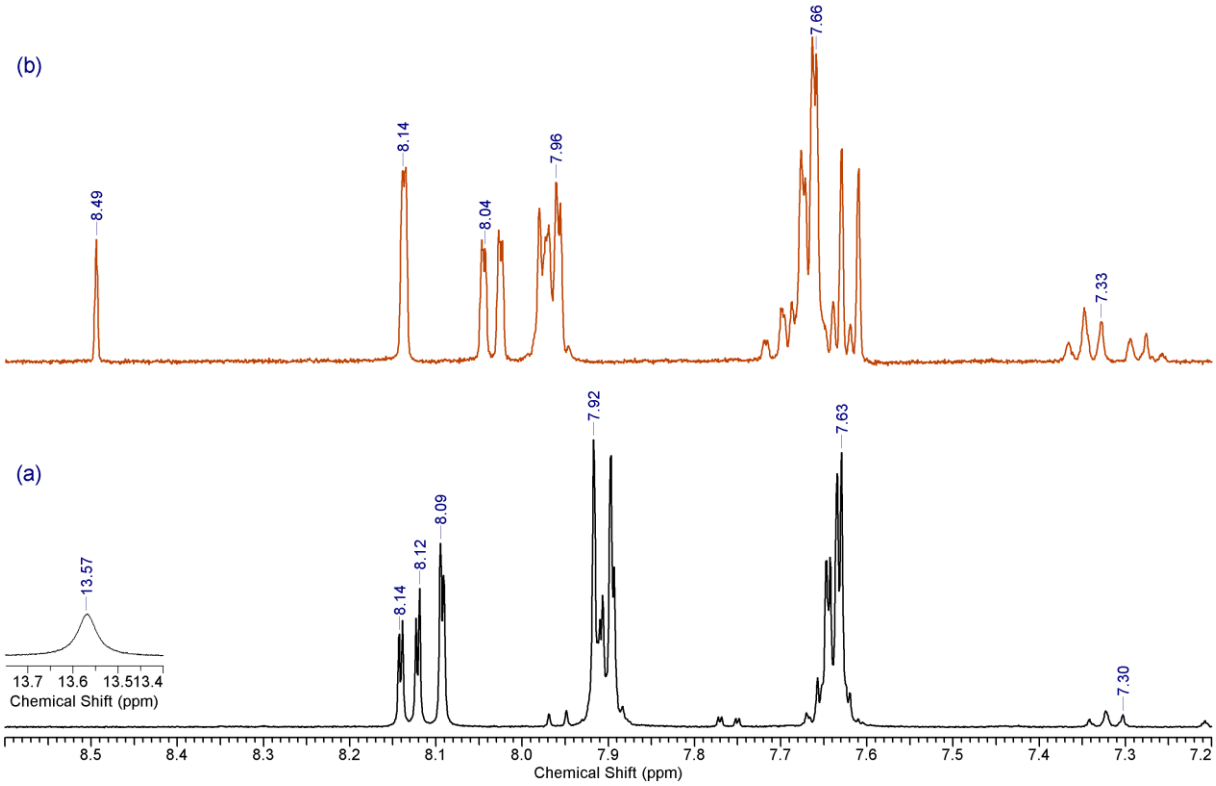

Fig. S1. ^{1}H NMR (400 MHz) of a) ligand [(*E*)-2-(phenyldiazenyl)terephthalic acid] in DMSO-d_6, and b) digested Azo-UiO-66 in the mixture solvent NaOD and D_2O.

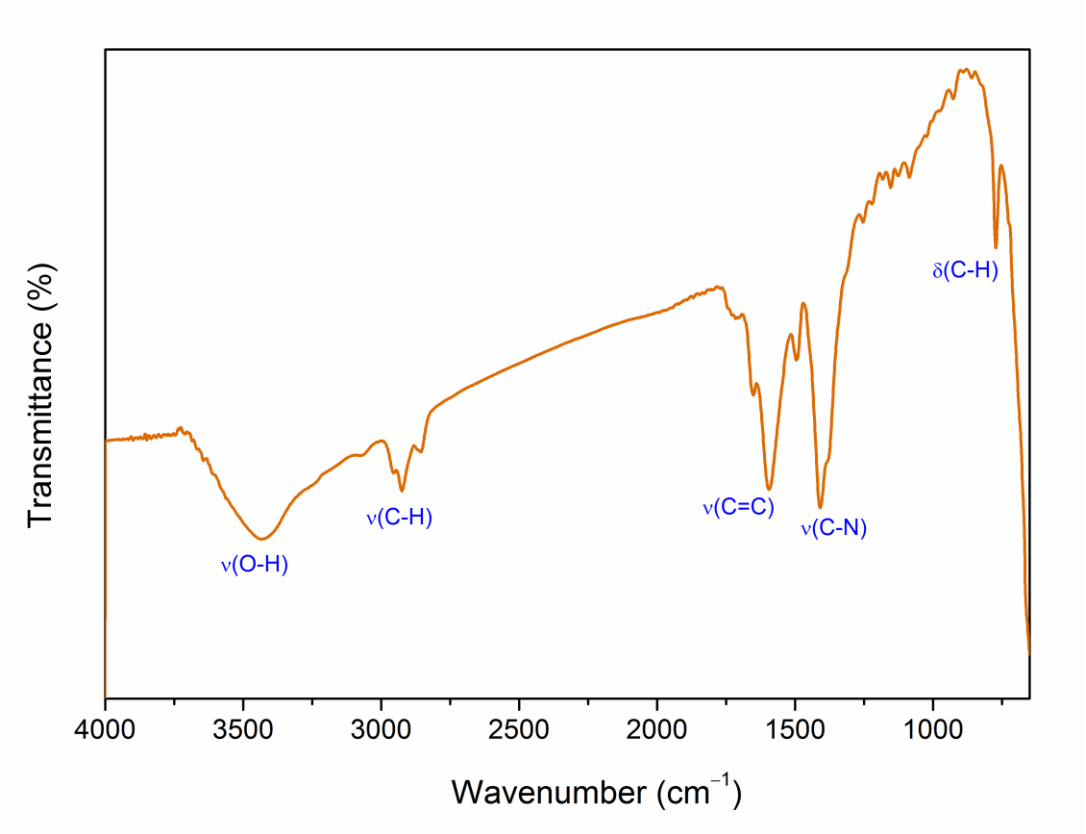

Fig. S2. FTIR spectrum of Azo-UiO-66.

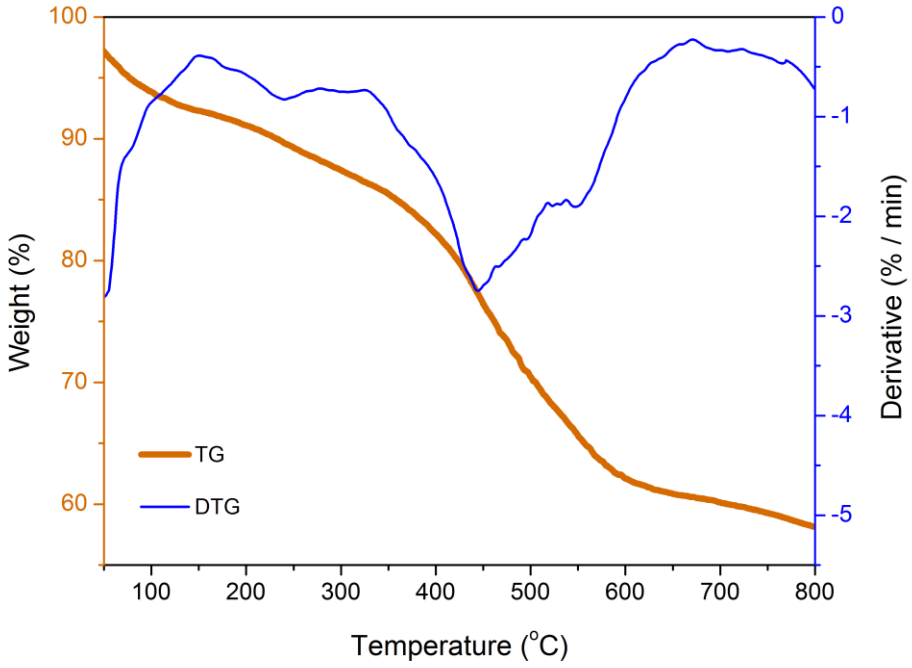

Fig. S3. TG and DTG curves obtained from Azo-UiO-66.

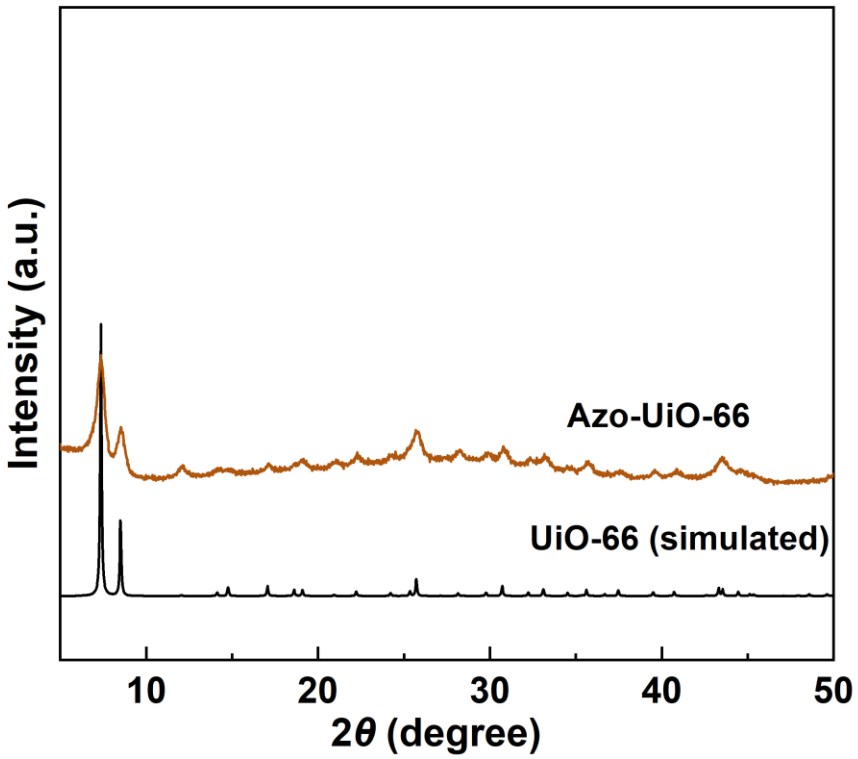

Fig. S4. Comparative XRD patterns of Azo-UiO-66 and simulated UiO-66**.**

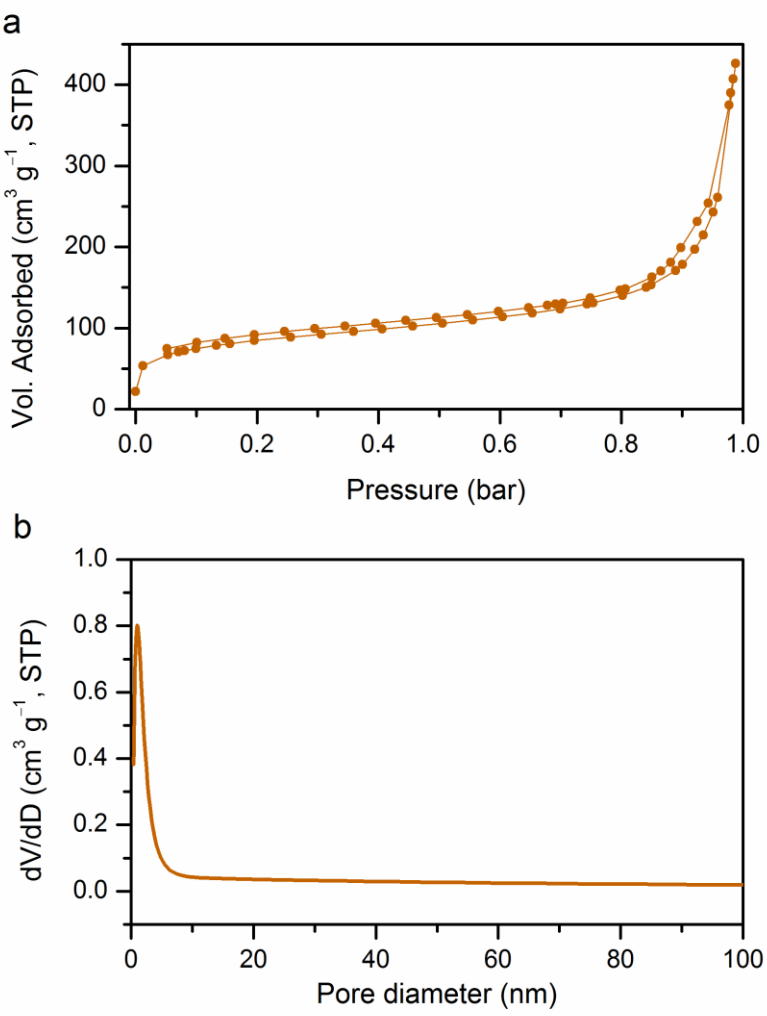

Fig. S5. (a) N_2 adsorption/desorption isotherm for determining the surface area (S_{BET}) of Azo-UiO-66 which is found to be 315.5 m^2 g^{-1}, and (b) Pore-size distribution of Azo-UiO-66 where the pore volume (V_p) and the pore-diameter (D_{micro}) are found to be 0.33 cm^3 g^{-1} and 0.65 nm.

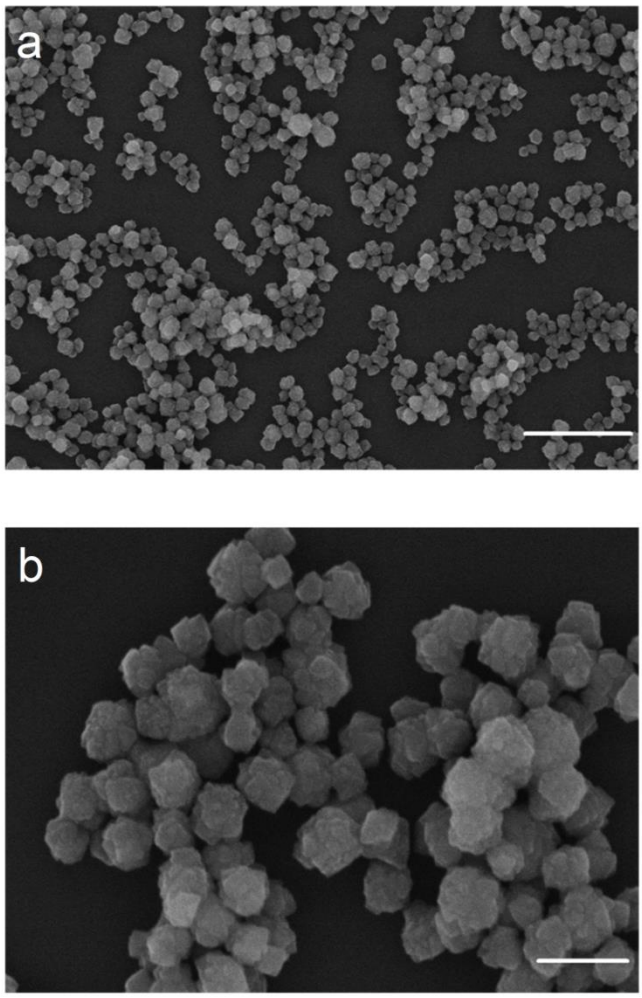

Fig. S6. SEM images with scales (a) 1.0 µm, and (b) 250 nm depicting octahedral-shaped Azo-UiO-66 nanoparticles.

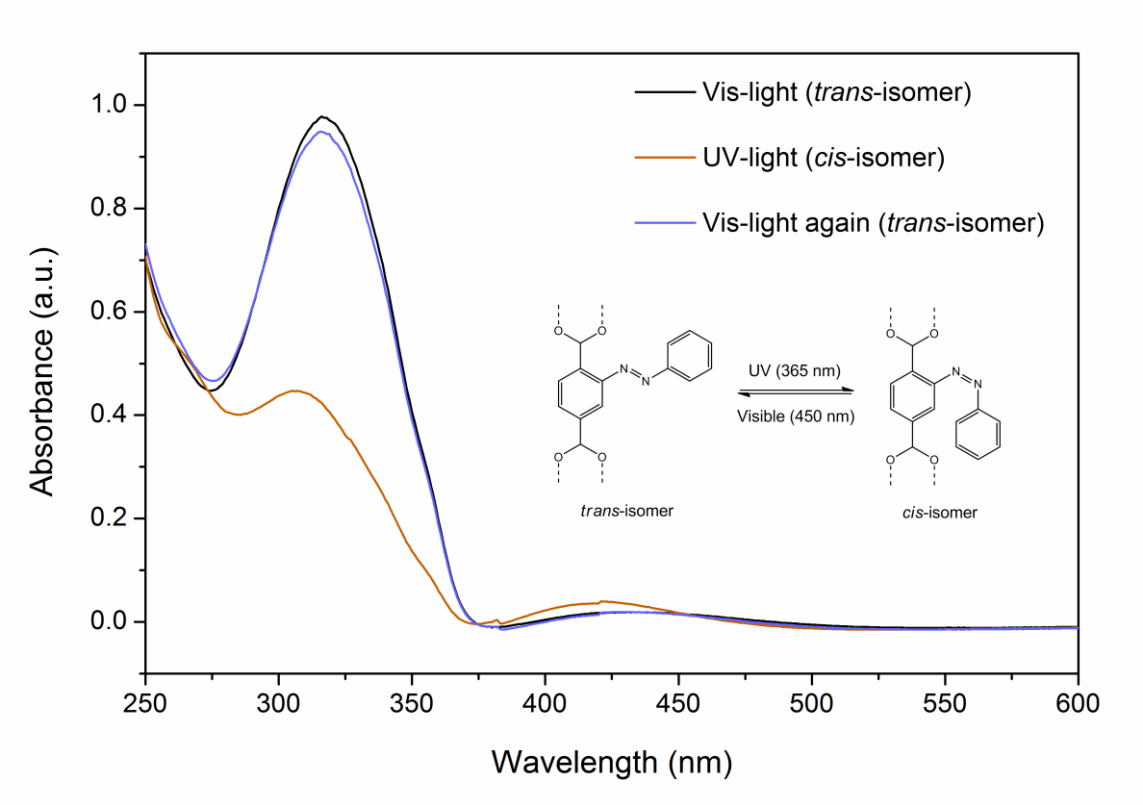

Fig. S7. UV/Vis analytical results of Azo-UiO-66 (dispersed in ethanol) exhibiting isomerization upon visible (420 nm; *trans*-isomer) and UV (365 nm; *cis*-isomer) light irradiation. The isomerization is reversible (*cis*- to *trans*-) by switching the light from UV to visible.

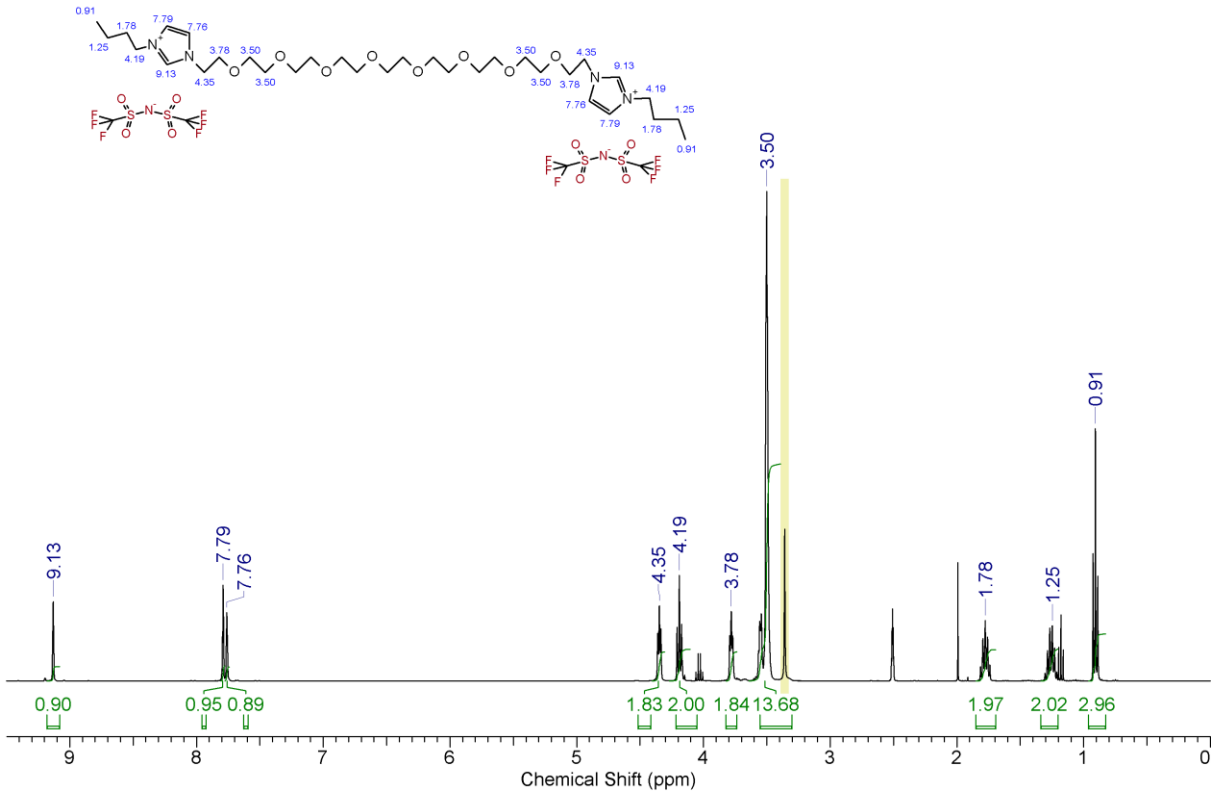

Fig. S8. ^{1}H NMR spectrum (400 MHz) of IL-NTf_2 in DMSO-d_6. The yellow shade peak in the spectrum belongs to the solvent (H_2O) as impurity.

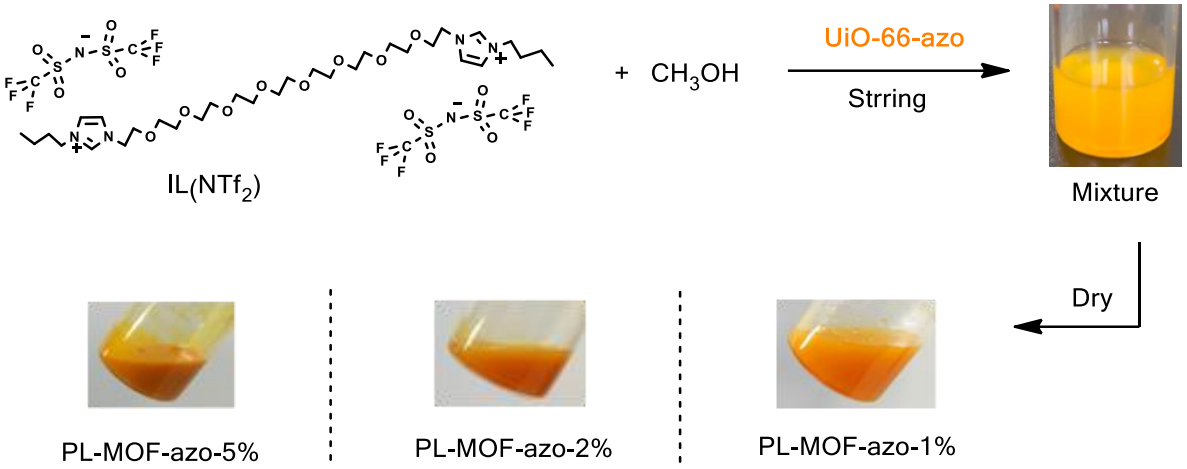

Fig. S9. Schematic representation for the synthesis of porous liquids (PL-MOF-azo-1%, 2% and 5%) by mixing 1%, 2% and 5% of Azo-UiO-66 in bulky IL-NTf_2. Methanol was used to reduce the viscosity of IL-NTf_2, and is further dried to obtain porous liquids.

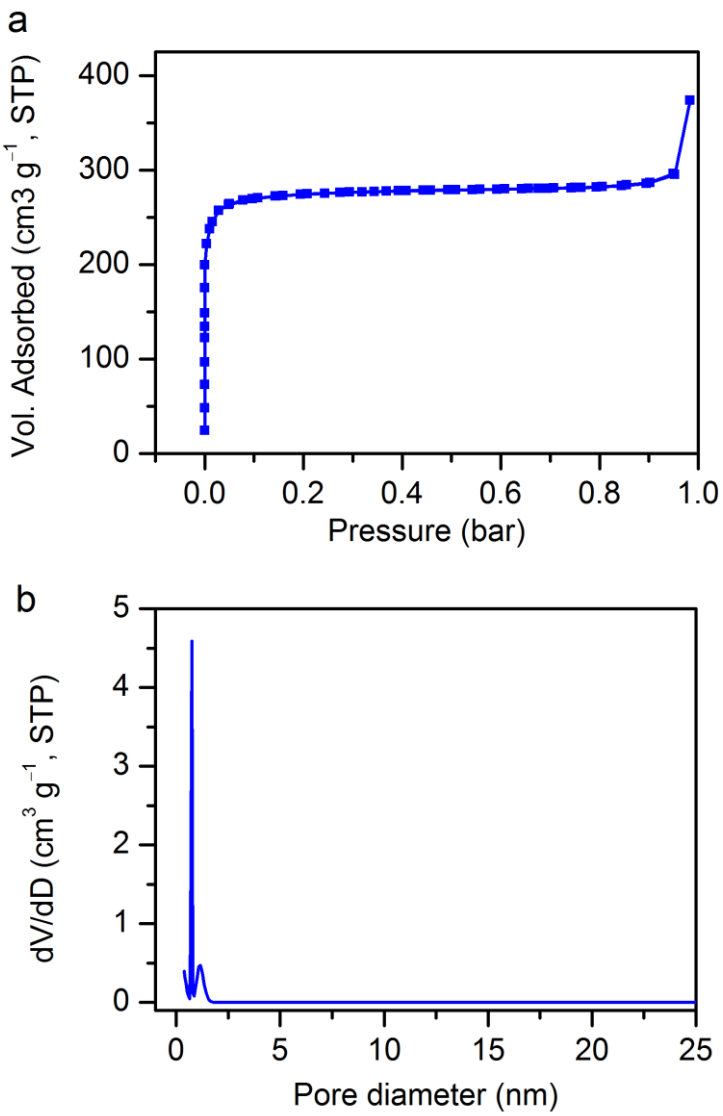

Fig. S10. (a) N_2 adsorption/desorption isotherm for determining the surface area (BET) of pristine UiO-66 which is 1088.7 m^2 g^{-1}, and (b) Pore-size distribution of pristine UiO-66 where the pore volume (Vp) is 0.73 cm^3 g^{-1} and the pore-diameters (Dmicro) are 0.56 and 1.63 nm.

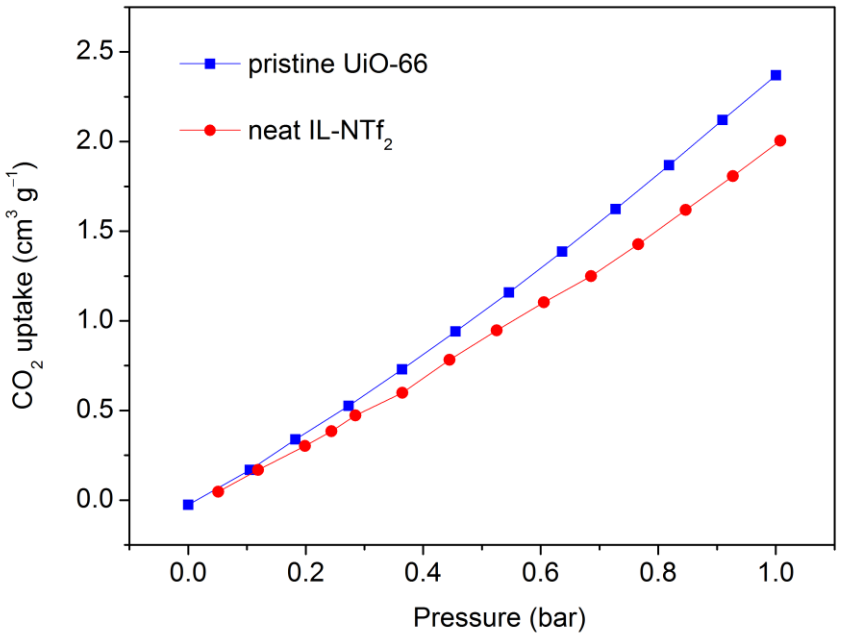

Fig. S11. CO_2 adsorption at 1 bar and 273 K by the mixture of UiO-66/IL-NTf_2 and neat IL-NTf_2. As can be seen, the compared gas adsorption results depict negligible differences. This indicates that the direct blending of UiO-66 with IL-NTf_2 create no cavity in the mixture as the IL molecule (size: 3.75 nm x 1.86 nm x 1.41 nm) can enter the pores of UiO-66 as per the pore-size distribution shown in Fig. S10.

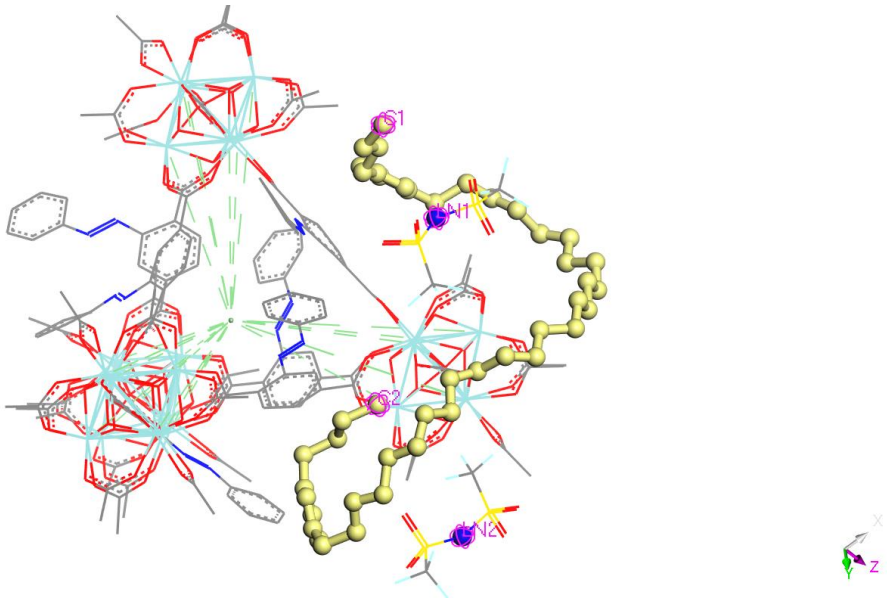

Fig. S12. Simulation to analyze the radial distribution functions between the centroid of the MOF cage and the two terminal carbon atoms of the cationic IL ligand and the two nitrogen atoms of the two IL anions. All hydrogen atoms are deleted for clarification purpose.

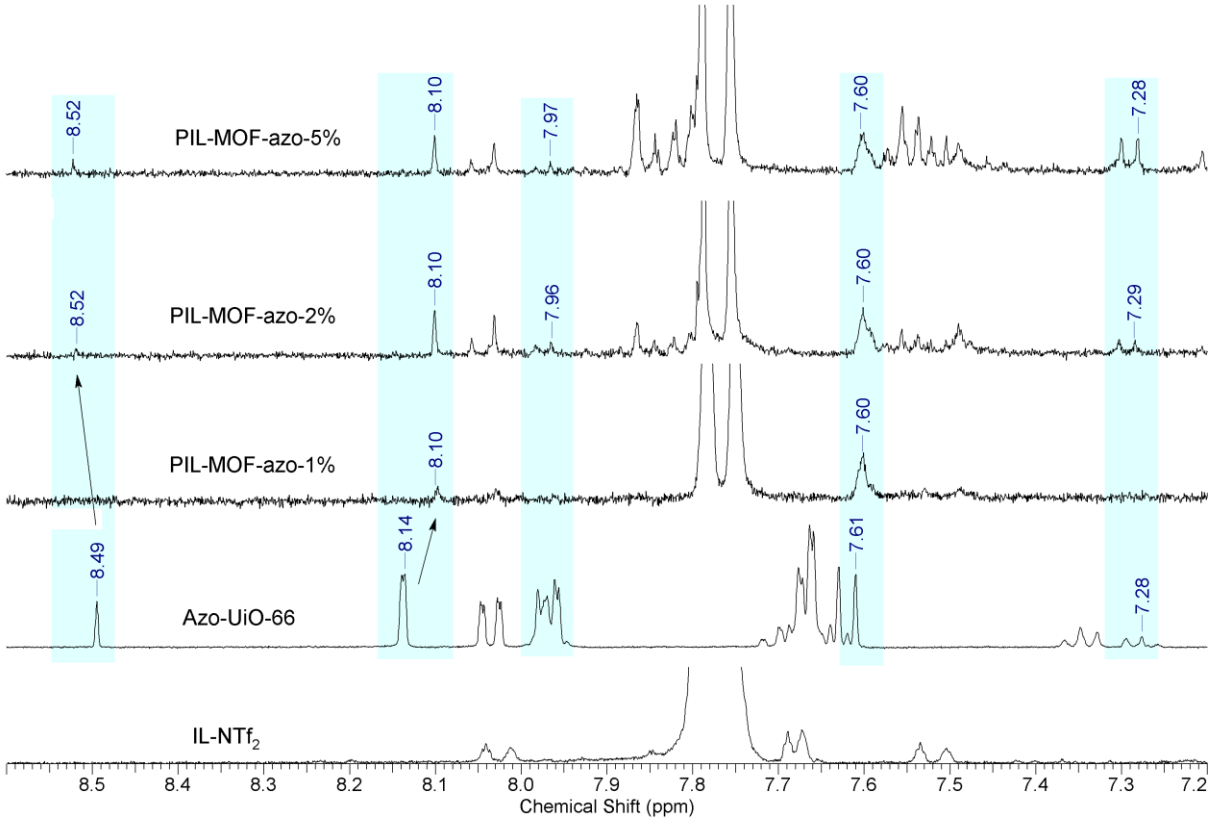

Fig. S13. Comparative ^{1}H NMR (400 MHz) spectra of neat IL-NTf_2 (DMSO-d_6), Azo-UiO-66 (NaOD + D_2O), PIL-MOF-azo-1% (NaOD + DMSO-d_6), PIL-MOF-azo-2% (NaOD + DMSO-d_6) and PIL-MOF-azo-5% (NaOD + DMSO-d_6).

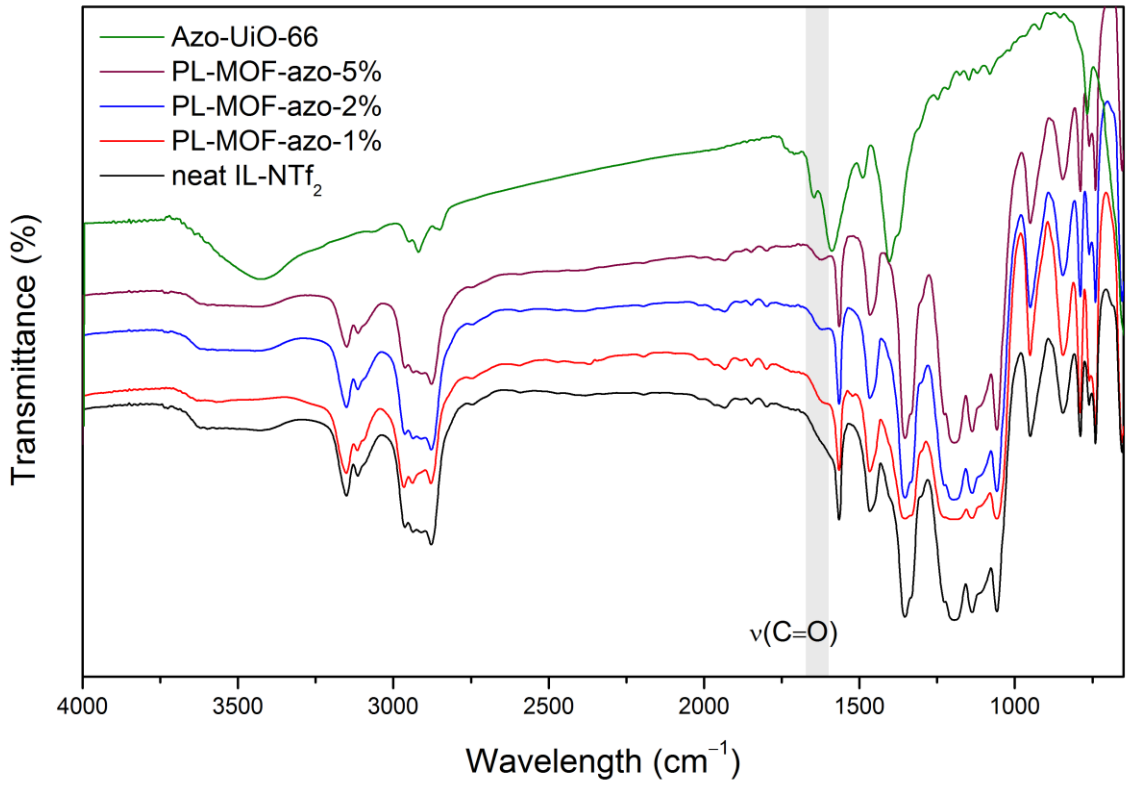

Fig. S14. Comparative FTIR spectra of neat IL-NTf_2, PIL-MOF-azo-1% PIL-MOF-azo-2% and PIL-MOF-azo-5%.

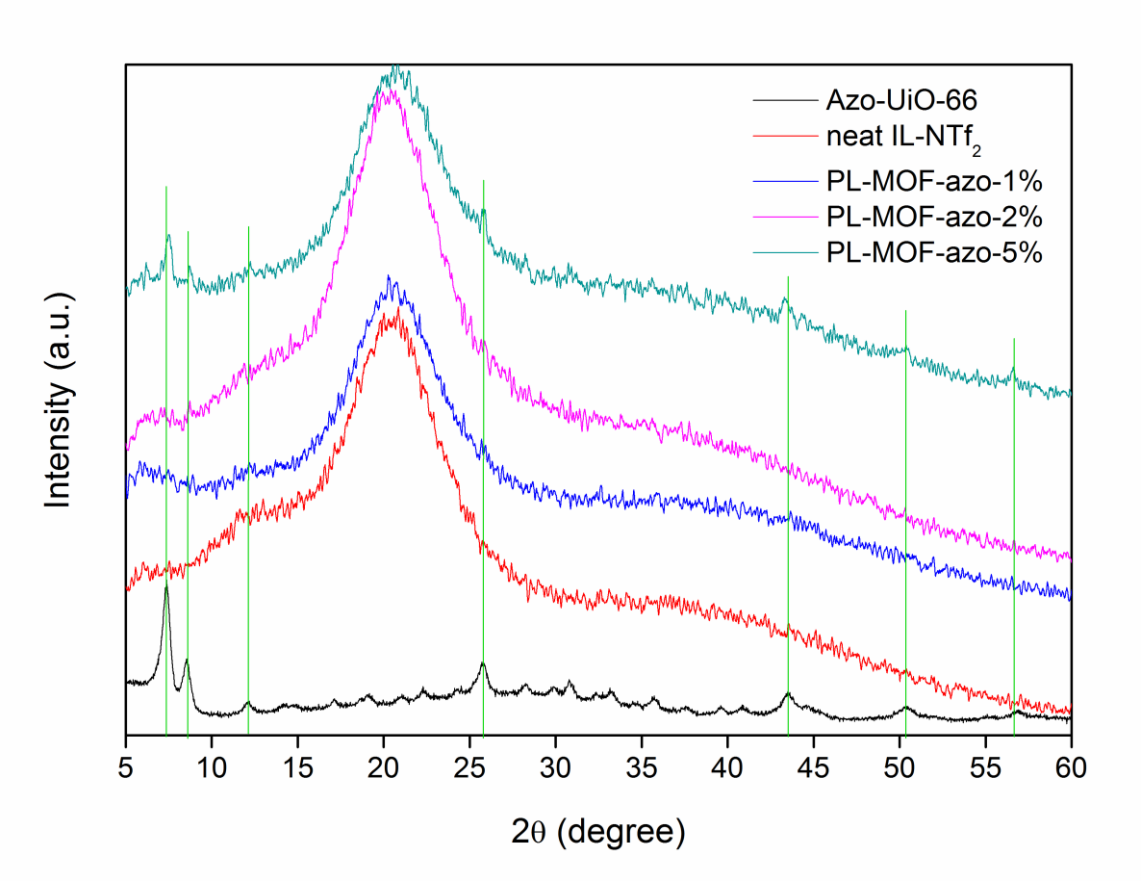

Fig. S15. Compared XRD patterns of neat IL-NTf_2 and Azo-UiO-66 with PL-MOF-azo-1, 2 and 5%.

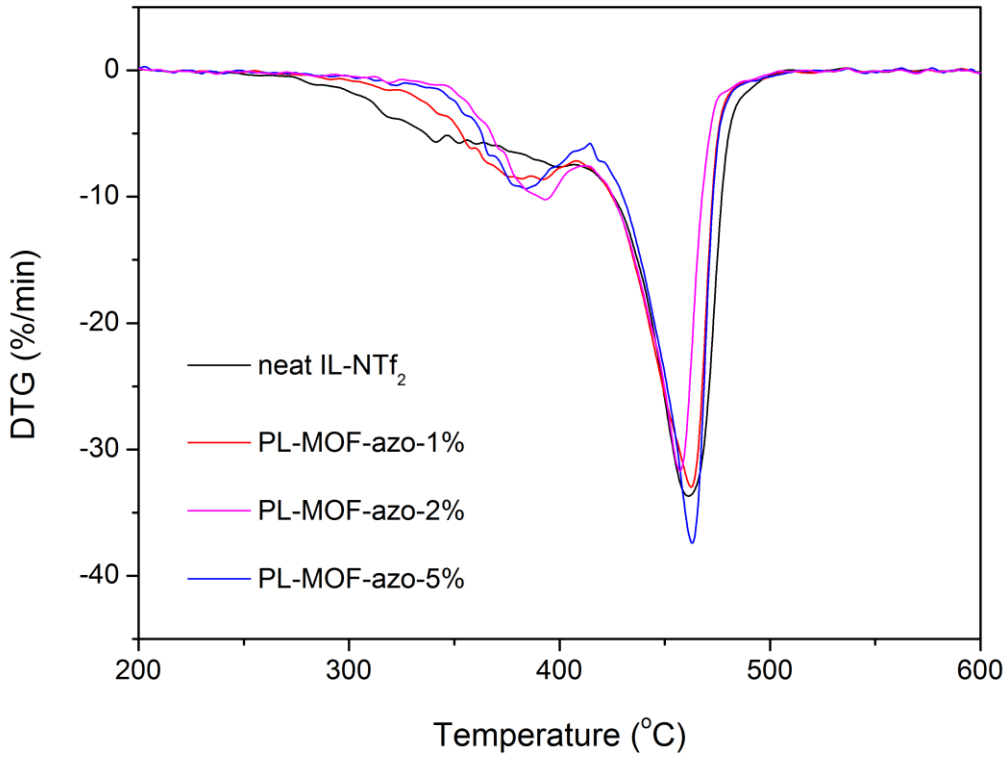

Fig. S16. Compared DTG analytical results from neat IL-NTf_2, and PL-MOF-azo-1, 2 and 5%.

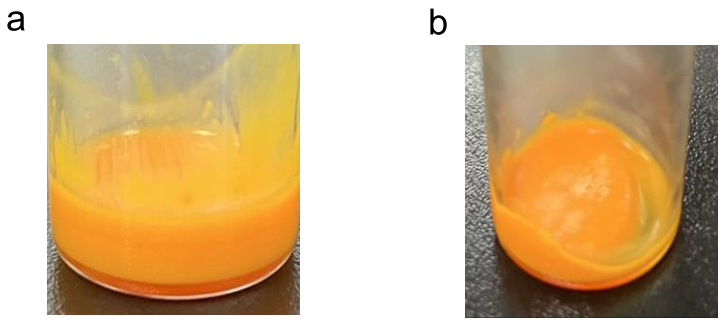

Fig. S17. Digital images of a) PL-MOF-azo-7%, and b) PL-MOF-azo-10%. These PLs are found to be highly viscous because of containing large content (saturation state) of Azo-UiO-66 and thus, difficult to utilize.

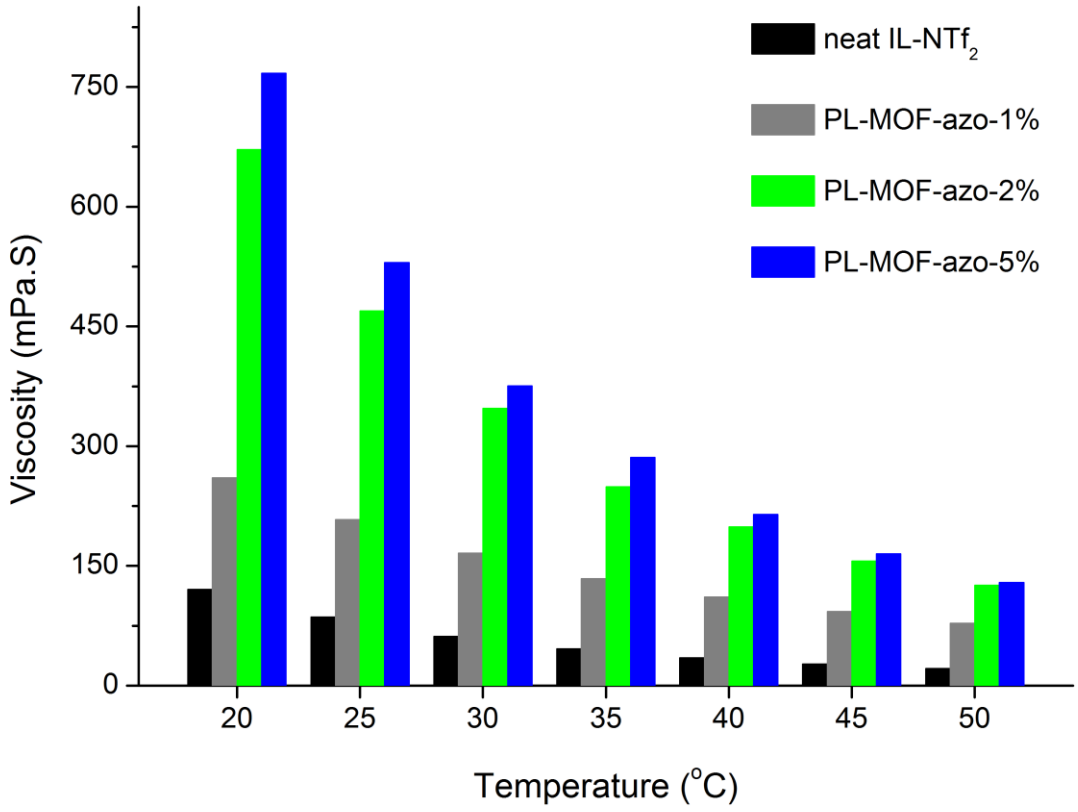

Fig. S18. Viscosity measurements of neat IL-NTf_2, PL-MOF-azo-1% PL-MOF-azo-2% and PL-MOF-azo-5%.

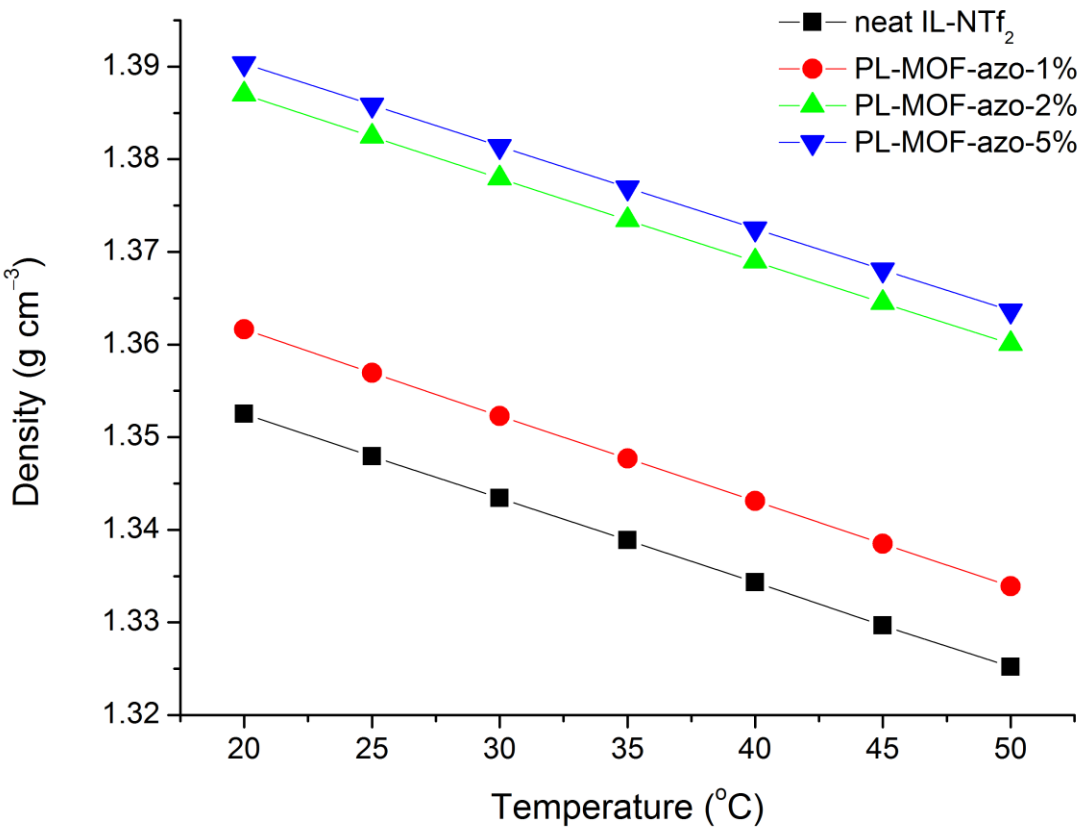

Fig. S19. Density measurements of neat IL-NTf_2, PL-MOF-azo-1% PL-MOF-azo-2% and PL-MOF-azo-5%.

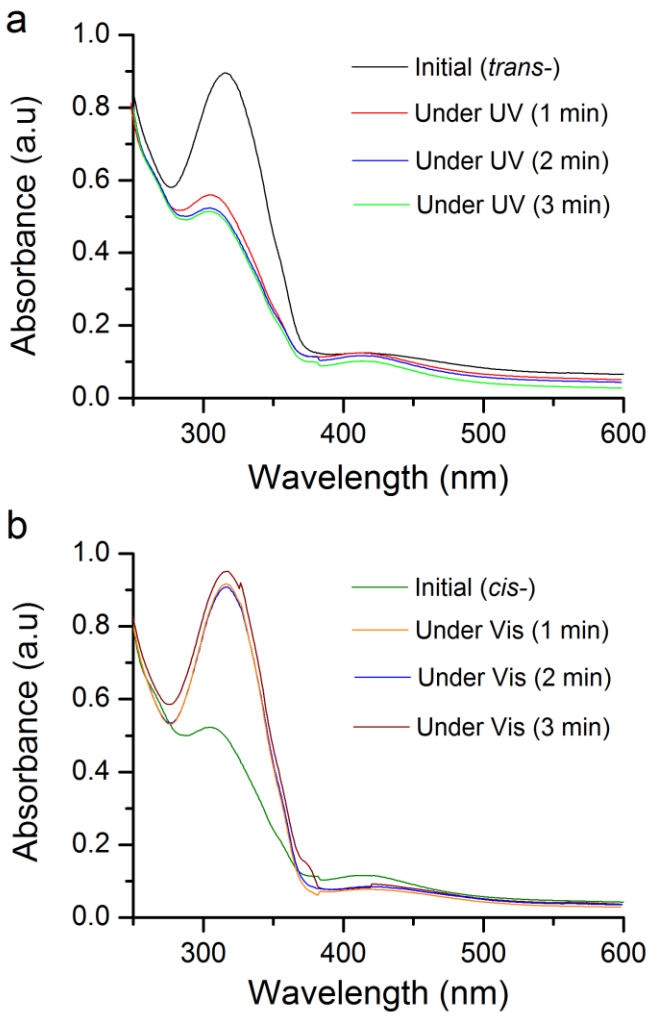

Fig. S20. UV-Vis spectra obtained of PL-MOF-azo-1% under a) UV-light (365 nm), and b) Vis-light irradiation (420 nm) after 1, 2 and 3 min.

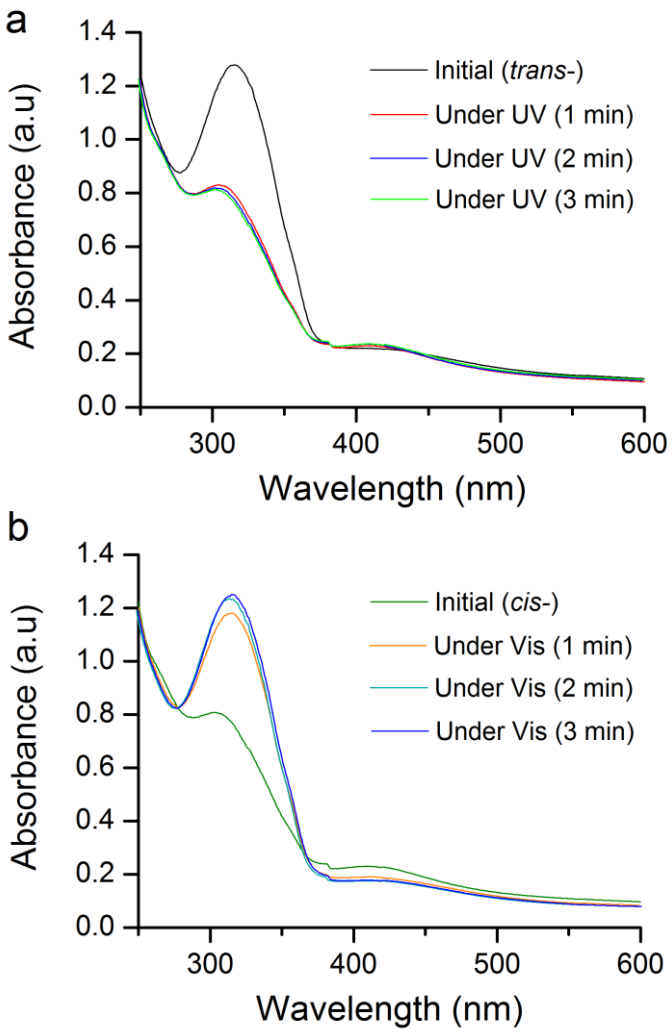

Fig. S21. UV-Vis spectra obtained of PL-MOF-azo-2% under (a) UV-light (365 nm), and (b) Vis-light irradiation (420 nm) after 1, 2 and 3 min.

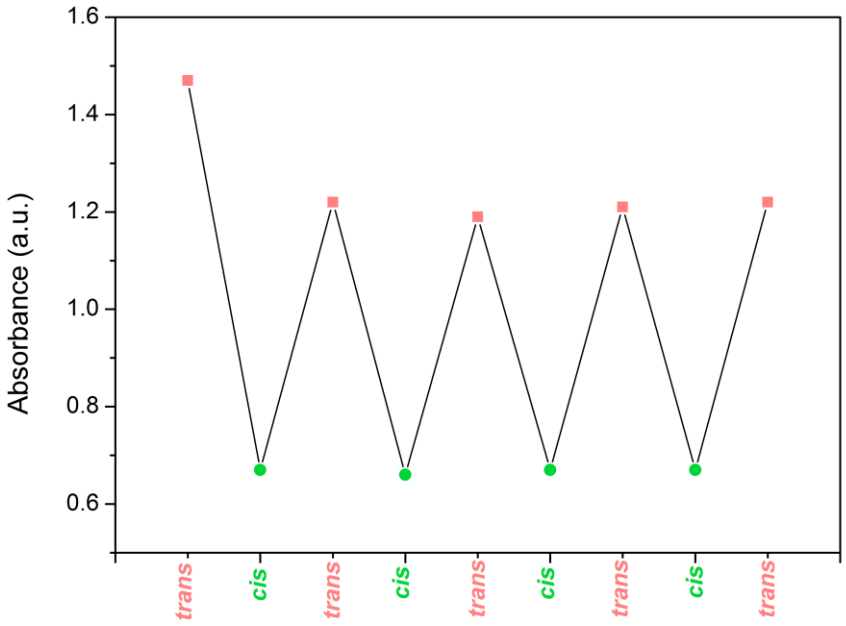

Fig. S22. Recyclable isomerization of PL-MOF-azo-5% upon irradiating under the visible and UV light periodically.

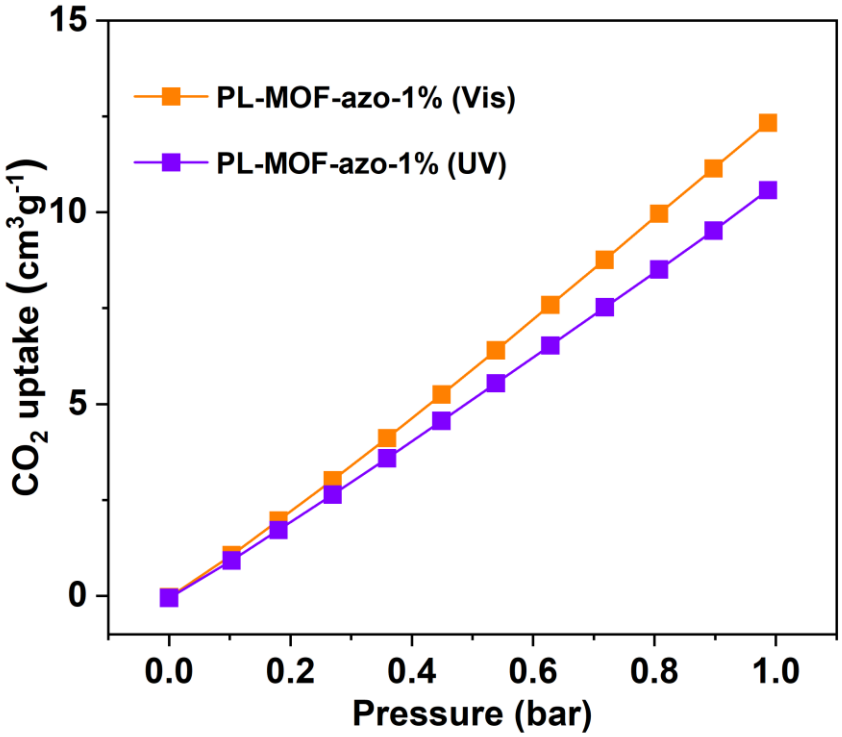

Fig. S23. Uptakes of CO_2 at 1 bar by PL-MOF-azo-1% under visible (420 nm) and UV-light (365 nm) irradiation.

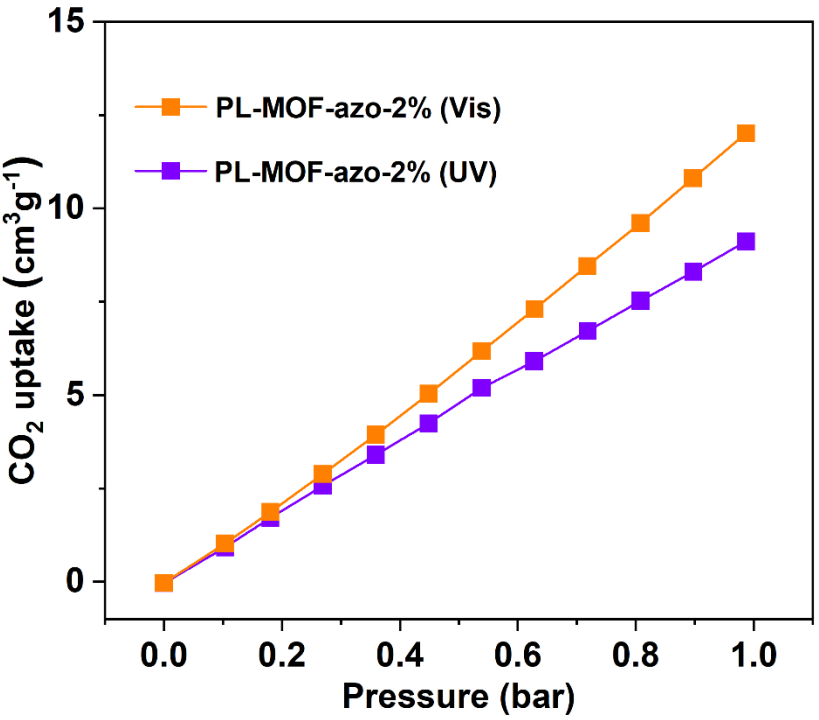

Fig. S24. Performance of PL-MOF-azo-2% under visible (420 nm) and UV-light (365 nm) on CO_2 adsorption at 1 bar.

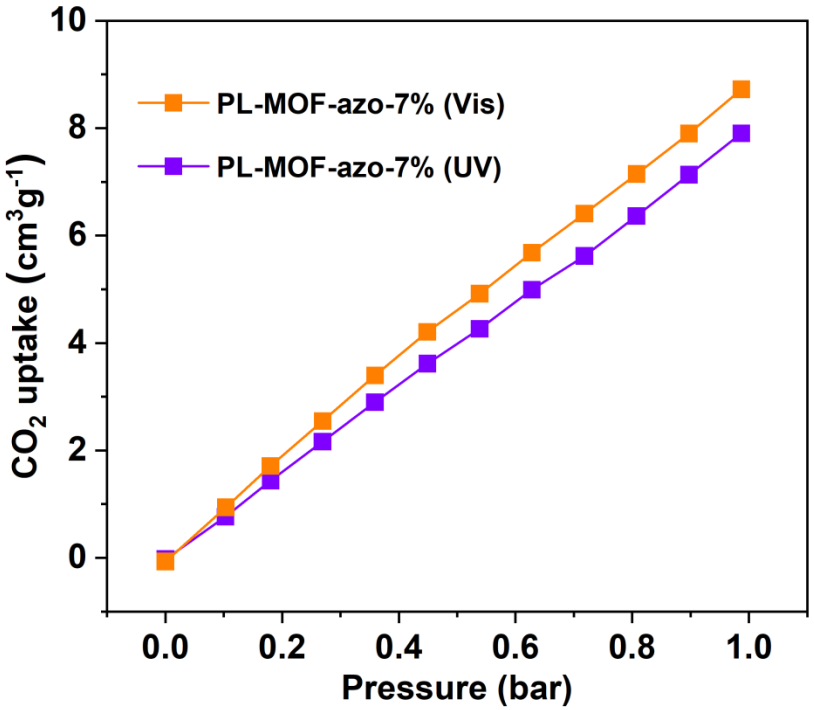

Fig. S25. Performance of PL-MOF-azo-7% under visible (420 nm) and UV-light (365 nm) on CO_2 adsorption at 1 bar. The change in CO_2 uptake is calculated to be merely 22%.

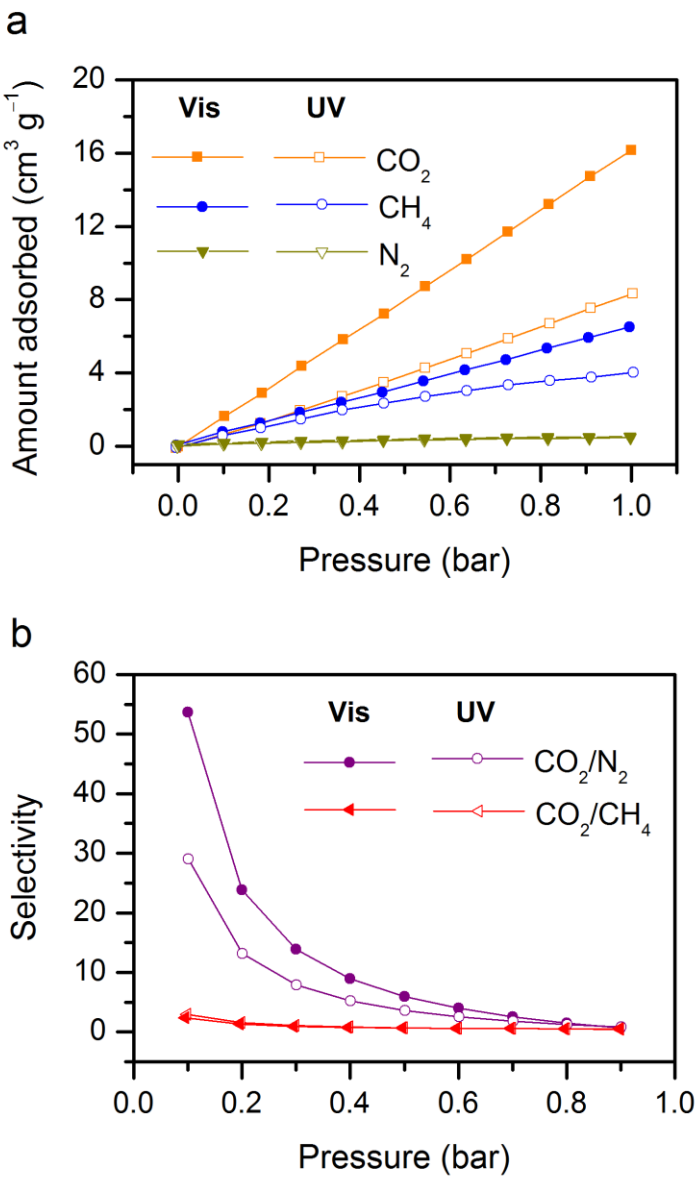

Fig. S26. (a) Adsorption behavior of PL-MOF-azo-5% for the gaseous molecules of CO_2, CH_4 and N_2 under visible and UV-light irradiation at 273 K. (b) Selectivity for CO_2/N_2 and CO_2/CH_4 by PL-MOF-azo-5% under UV/Vis light at 273 K.

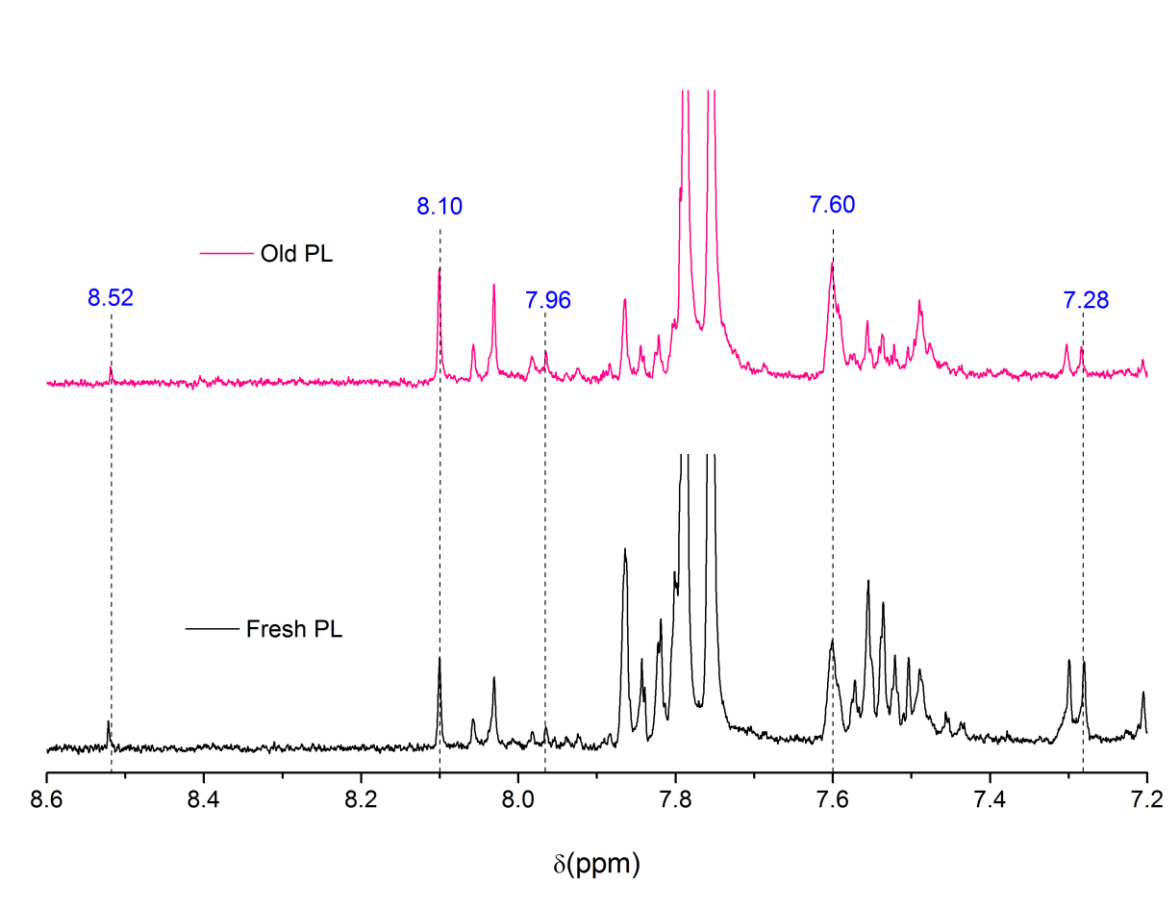

Fig. S27. Compared ^{1}H NMR spectra of fresh and six month old sample of PL-MOF-azo-5%.

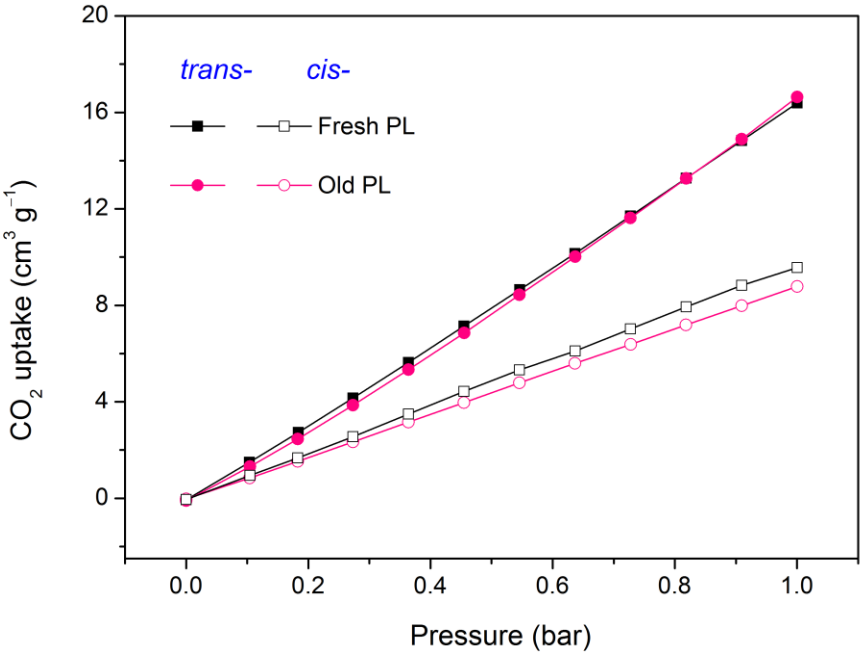

Fig. S28. Adsorption behavior of fresh and six months old sample of PL-MOF-azo-5% for CO_2 under visible and UV light irradiation at 273 K.

Section 3. Supporting Tables

Table S1. Comparative adsorption capacities of reported porous liquids with PL-MOF-azo-5% for CO_2 at 273 K and various pressures**.**

Porous liquid	**Type**	**Porous host**	**CO_2 uptake ($cm^3\ g^{-1}$)**	**Pressure（bar）**	**Reference**
PL-MOF-azo-5%	III	Azo-UiO-66	16	1	This work
PIL-*diz*-RhMOP	II	*diz*-RhMOP	2.97	1	[4]
Gel-IL	II	Gel	1.45	1	[5]
5-30TEPA@ZIF-8/[EMlm][NTf_2]	III	ZIF-8	2.78	1	[6]
Im-PL-Cage	I	Zn-Cage	39.87	10	[7]
P-UiO-66-PLs	III	P-UiO-66	39.61	10	[8]
ZIF-8/[DBU-PEG][NTf_2]	III	ZIF-8	34.94	10	[9]
PIL-**1**-2%	II	PdMOP	19.98	10	[10]

References

1. G. Cai, H. L. Jiang, *Angew. Chem. Int. Ed.* 2017, **56**, 563–567.
2. A. K. Rappé, C. J. Casewit, K. S. Colwell, W. A. Goddard and W. M. Skiff, *J. Am. Chem. Soc.* 1992, **114**, 10024–10035.
3. D. Dubbeldam, S. Calero, D. E. Ellis, R. Q. Snurr, *Mol. Simul.* 2016, **42**, 81–101.
4. M. K. Dinker, M. M. Li, K. Zhao, M. Zuo, L. Ding, X. Q. Liu, L. B. Sun, *Angew. Chem. Int. Ed.* 2023, **62**, e202306495.
5. Z. Wang, A. Ozcan, G. A. Craig, F. Haase, T. Aoyama, D. Poloneeva, K. Horio, M. Higuchi, M. S. Yao, C. M. Doherty, G. Maurin, K. Urayama, A. Bavykina, S. Horike, J. Gascon, R. Semino, S. Furukawa, *J. Am. Chem. Soc.* 2023, **145**, 14456–14465.
6. X. Zhao, Y. Ding, L. Ma, X. Zhu, H. Wang, M. Cheng, Q. Liao, *Energy* 2023, **279**, 127975.
7. C. He, Y. H. Zou, D. H. Si, Z. A. Chen, T. F. Liu, R. Cao, Y. B. Huang, *Nat. Commun.* 2023, **14**, 3317.
8. Y. Xin, H. Ning, D. Wang, X. Li, W. Fan, X. Ju, H. Wang, Y. Zhang, Z. Yang, D. Yao, Y. Zheng, *Nano Res.* 2023, **16**, 10369–10380.
9. X. Zhao, Y. Ding, L. Ma, X. Zhu, H. Wang, Q. Liao, *J. Mol. Liq.* 2022, **367**, 120523.
10. M. K. Dinker, K. Zhao, S. Liu, S. C. Qi, Y. X. Li, G. P. Liu, L. Ding, X. Q. Liu, L. B. Sun, *J. Mater. Chem. A* 2022, **10**, 16204–16211.